Investigating the Order Parameters of Saturated Lipid Molecules under Various Curvature Conditions on Spherical Supported Lipid Bilayers

ARTICLE *in* THE JOURNAL OF PHYSICAL CHEMISTRY B · MARCH 2015

Impact Factor: 3.3 · DOI: 10.1021/jp510322t · Source: PubMed

3 AUTHORS, INCLUDING:

Bocheng Yin

University of Pittsburgh

6 PUBLICATIONS **54** CITATIONS

THE JOURNAL OF PHYSICAL CHEMISTRY B

Article

pubs.acs.org/JPCB

Investigating the Order Parameters of Saturated Lipid Molecules under Various Curvature Conditions on Spherical Supported Lipid Bilayers

Lauren E. Marbella,* Bocheng Yin, and Megan M. Spence

Department of Chemistry, University of Pittsburgh, Pittsburgh, Pennsylvania 15260, United States

Supporting Information

ABSTRACT: The conformations and motions of lipid molecules under different membrane curvatures have important implications for transmembrane protein function, binding events, and overall membrane organization. This work reports on the local order parameters of saturated lipid molecules, as measured by ^{13}C NMR relaxation, under several curvature conditions to probe structural changes as a function of lipid bilayer curvature. Different curvature conditions are created by depositing phosphatidylcholine membranes on spherical beads of various diameters. The findings reveal that the order parameters are not a continuous function of the membrane curvature. While small (30 nm) and large (110 nm) diameter bilayers exhibit similar order parameters, bilayers with curvatures of 60−80 nm diameter show a consistently increased order parameter along the entire lipid molecule, indicating a higher packing density and lateral tension. Order parameters for curvatures between 60 and 80 nm also show molecular evidence for interdigitation.

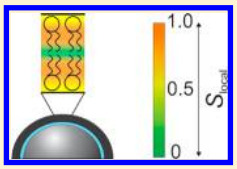

INTRODUCTION

Membrane curvature is believed to play an important role in cell biology. All membranes have an inherent curvature that is the result of a unique, diverse mixture of lipid molecules and proteins that perform specific biological functions.[1] The presence of highly curved membranes is evident in different organelles and throughout biological processes, as illustrated in Figure 1.[2−6] Diameters of curvature typically range from 20 to

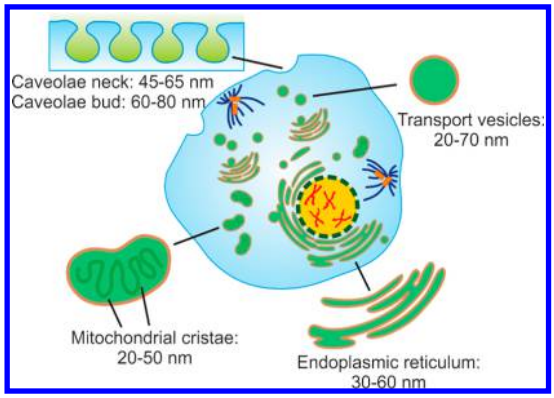

Figure 1. Static structure of cellular organelles and their respective diameters.

100 nm. For example, the cross-sectional diameters of cristae in mitochondria tend to be ∼20−50 nm, depending on the organism and the cell type.[2,5] Due to the length scale of cell membranes (on the order of micrometers), small molecules and proteins typically view the local environment of the bilayer as planar. However, alterations in membrane curvature, such as the formation of small caveolae with diameters of 45−65 nm at the neck of the bulb that occur during budding events,[3] indicate that transient changes in curvature can change this view and have an effect on certain biological events.

This vital bending of the membrane is achieved through a delicate balance of lipid and protein interactions and arises dynamically during cellular activity. Bilayer deformation commonly occurs in response to the insertion of small molecules[7] and proteins,[8−11] leading to changes in membrane shape, such as raft formation effects.[12−18] Often, changes in membrane morphology, such as curvature, are energetically unfavorable because hydrophobic regions are exposed to water. To reduce the unfavorable energy of the highly curved state, the membrane forms defects which can play a significant role in membrane function. For example, molecular dynamics (MD) simulations show that other lipids, in addition to small molecules and proteins, can selectively bind to these defects. Remarkably, in an effort to reduce exposure of the hydrophobic core to the surrounding water, lipids were also shown to flip-flop between the inner and outer leaflets of the bilayer to produce the tightest packing of the headgroups.[19] Furthermore, in order to provide additional stability, the acyl tails of polyunsaturated lipids can fold back on themselves to reduce the surface area of exposed hydrophobic regions in the outer leaflet under high curvature conditions.[19] Compensation for membrane defects was also experimentally observed in saturated 1,2-dimyristoyl-*sn*-glycero-3-phosphocholine (DMPC) coated silica nanobeads, which provide a method to easily control curvature in model systems. For small diameters, the hydrocarbon chains of the supported lipid bilayers have highly ordered trans chain conformations.[20] As the bead

Received: October 13, 2014
Revised: February 17, 2015
Published: March 10, 2015

DOI: 10.1021/jp510322t
J. Phys. Chem. B 2015, 119, 4194−4202

diameter is increased, the alkyl chains become increasingly disordered in terms of lateral packing and gauche defects.[20]

Measuring the local dynamics and order parameters of individual segments of lipid molecules can provide critical information about the structural rearrangement encountered by a membrane under different degrees of curvature. Deuterium NMR has a long history of probing the segmental order parameters of lipids with a high degree of accuracy.[21−34] More recently, techniques such as $^{1}H-^{13}C$ dipolar recoupling NMR[35−39] and ^{13}C NMR relaxation[40−42] measurements eliminate the need for isotopic labeling and can extract lipid order parameters at natural abundances with accuracy comparable to ^{2}H NMR and spin-labeled EPR. Furthermore, with advances in computational methodology, lipid order parameters can be simulated to provide complementary information.[43−45] A recent review tabulates and compares the aforementioned NMR techniques to computer simulations, providing a convenient database for such studies.[46]

In this work, we examine the local order parameters of saturated phosphatidylcholine membranes under various curvature conditions to evaluate structural changes induced by increasing the curvature of a lipid bilayer. To probe the effect of curvature changes on lipid bilayers, we used ^{13}C NMR relaxation to provide information on the local dynamic motion on the picosecond to nanosecond time scale[47,48] to obtain the order parameters (S_{C-H}) for each carbon segment in the lipid molecule. Since supported lipid bilayers have been successful in previous NMR studies,[21,49,50] we chose to use spherical, supported phosphatidylcholine vesicles[51] as a platform to maintain direct control over the degree of curvature experienced by the bilayer. The inner diameter of the membrane was varied from 20 to 100 nm, and different intermediate sizes were also sampled to provide a size range comparable to curvatures commonly encountered in biological membrane systems.[4] Here, silica beads serve as a nanoscale template that creates a monodisperse sample of supported membranes with different curvatures.[52] From the extracted order parameters, we observe changes in membrane structure that change as a function of curvature. We suggest that these structural changes are consistent with lipid chain interdigitation, and we examine its potential impact.

EXPERIMENTAL SECTION

Materials. 1,2-Dimyristoyl-*sn*-glycero-3-phosphocholine (DMPC, >99%) powder was purchased from Avanti Polar Lipids (Alabster, AL) and used as received. SNOWTEX colloidal silica beads with diameters of (i) 10−20 nm, commercial lot number ST-40, 40−41 wt % SiO_2, $\rho_{solution}$ = 1.28−1.35 g/cm^3; (ii) 20−30 nm, ST-50, 47−49 wt % SiO_2, $\rho_{solution}$ = 1.36−1.40 g/cm^3; (iii) 40−50 nm, ST-OL, 20−21 wt % SiO_2, $\rho_{solution}$ = 1.12−1.14 g/cm^3; and (iv) 70−100 nm, ST-ZL, 40−41 wt % SiO_2, $\rho_{solution}$ = 1.29−1.32 g/cm^3 were received from Nissan Chemical America Corp. as a gift. Deuterium oxide (99.9%) was obtained from Cambridge Isotope Laboratories, Inc. (Andover, MA). NaCl was purchased from Fisher Scientific (Fair Lawn, NJ) and used as received.

Silica Bead Purification. The colloidal SiO_2 beads were purified by centrifugation to selectively separate beads of the desired size from each raw sample. First, a volume of the as-received SiO_2 beads was diluted with an equal volume of 0.5 mM NaCl. Monodisperse beads were obtained by centrifugation at an optimized speed and time: (i) 20 nm SiO_2 beads were obtained from ST-40 by centrifugation at 20000*g* for 20 min intervals until no pellet was obtained; (ii) 30 nm SiO_2 beads were obtained from ST-50 by centrifugation at 20000*g* for 20 min intervals until no pellet was obtained; (iii) 50 nm SiO_2 beads were obtained from ST-OL by centrifugation at 10000*g* for 20 min intervals until no pellet was obtained; (iv) 60 nm SiO_2 beads were obtained from ST-OL by centrifugation at 12000*g* for 10 min intervals until no pellet was obtained; (v) 100 nm SiO_2 beads were obtained from ST-ZL by centrifugation at 4170*g* for 5 min intervals until no pellet was obtained. Dynamic light scattering (DLS) was performed on all centrifuged portions to confirm the samples were the correct size and of suitable monodispersity. After this purification procedure, SiO_2 beads with diameters of approximately 20, 30, 50, 65, and 100 nm with narrow population distributions (size deviation <5 nm) were extracted from the raw commercial products ST-40, ST-50, ST-OL, and ST-ZL, respectively.

Lipid Vesicle Preparation. DMPC powder was dispersed in 0.5 mM NaCl and incubated at 60 °C for 2 h with intermittent vortexing to produce multilamellar vesicles (MLVs). The resulting MLVs were downsized using a mini extruder (Avanti Polar Lipids, Inc.) and passed through a polycarbonate membrane with a pore size of 100 nm, at 60 °C. The process was repeated 21 times to produce large unilamellar vesicles (LUVs) with a diameter of 100 nm, which was confirmed by DLS. To ensure that the lipid bilayers maintained their original fluidity and functionality even though they were bound to SiO_2 beads, we also performed NMR analysis on 100 nm LUVs in the absence of a solid support.

Lipid Coated Bead Preparation. We followed a previously reported procedure[52] to fabricate lipid coated beads in a dilute, aqueous environment. Additional modifications were made to concentrate the sample for ^{13}C NMR measurement. The necessary amount of lipids and SiO_2 beads was carefully calculated to ensure that only a single bilayer of lipid was deposited on the SiO_2 bead. The surface area ratio of lipid bilayer (A_L) to bead (A_B) was set equal to 1. The bead and lipid solution was diluted with 0.5 mM NaCl to obtain a final lipid concentration of 2 mg/mL. Thin layer chromatography was performed to compare multilamellar DMPC vesicles, 100 nm unilamellar DMPC vesicles, and DMPC-coated beads of approximately 30, 45, 60, 75, and 110 nm diameters. The samples were spotted on the TLC plate and separated in a chloroform/methanol/water 60/30/5 mixture by volume. No change was observed between the three samples, indicating that lyso-PC was not formed as a result of depositing the bilayers on SiO_2 beads. It should be noted that the following formulation and concentration of lipid coated beads (LCBs) is intricate and is extremely sensitive to ionic concentration and centrifugal force.

Small Lipid Coated Beads (from 20 and 30 nm SiO_2 Beads). The purified SiO_2 bead solution (described under Silica Bead Purification) and 6 mL of the 20 mg/mL extruded lipid vesicle solution (described under Lipid Vesicle Preparation) were combined for a total volume of 60 mL (final DMPC concentration = 2 mg/mL and the SiO_2 bead concentration varied, depending on the surface area of each size, vide supra) in a vial and stirred at 50 °C for 48 h. The sample was then removed from the heat and stirred for an additional 12−24 h at room temperature. The resulting LCBs were concentrated via centrifugation in Amicon Ultra Centrifugal Filters (Millipore, Ltd.) at 5000*g* for 10 min. The concentrated LCBs were then washed and resuspended in D_2O to obtain a final volume of 1

DOI: 10.1021/jp510322t
J. Phys. Chem. B 2015, 119, 4194−4202

mL. A 500 μL volume of this solution was loaded into a 5 mm NMR tube.

Large Lipid Coated Beads (from 50 to 100 nm SiO_2 Beads). The purified SiO_2 bead solution and 6 mL of the 20 mg/mL extruded lipid vesicle solution was combined in a vial for a final volume of 60 mL (final DMPC concentration = 2 mg/mL and the SiO_2 bead concentration varied, depending on the surface area of each size, vide supra) stirred at 50 °C for 12 h, followed by stirring at room temperature for 30 min. The resulting LCBs were concentrated by centrifugation at 5000*g* for 50 nm beads, 4500*g* for 60 nm beads, and 4170*g* for 100 nm beads for 10 min each. The concentrated LCBs were then washed and resuspended in D_2O for a final volume of 1 mL. A 500 μL volume of this solution was loaded into a 5 mm NMR tube.

DLS and TGA Analysis. The size and polydispersity of all LCBs described above were confirmed by DLS on a particle size analyzer (Brookhaven Instruments Corp.), using a 90° scattering detection angle at 25 °C in water. The lipid coating efficiency[51] on SiO_2 beads was measured by thermal gravimetric analysis (TGA) on a TGA Q500 (TA Instruments, Waters LLC, New Castle, DE). TGA data were collected from 20 to 800 °C. The TGA and DLS analysis indicated single-bilayer deposition on the SiO_2 beads. The coverage weight percentage is given by eq 1:

$$\text{coverage weight \%} = \left[1 - \left(\frac{m_B}{m_B + m_L}\right)\right]\cdot 100\% \tag{1}$$

where m_B is the mass of the SiO_2 beads and m_L is the mass of the lipids. The calculated coverage percentage was predicted by computing the mass of the lipids from eq 2:

$$m_L = \frac{2A_B M_L m_B}{A_L SG_B V_B} \tag{2}$$

where A_B is the surface area of the bead calculated from the radius, M_L is the molecular weight of DMPC = 677.94 g/mol, A_L is the surface area occupied by one DMPC molecule = 55 Å^2, SG_B is the specific gravity of the beads, and V_B is the volume occupied by one bead of a particular radius. The factor of 2 arises from the need to account for both sides of the bilayer.

NMR Spectroscopy. All ^{13}C NMR experiments were acquired on a Bruker 500 Ultrashield Magnet with an AVANCE III Console and a Bruker 600 Ultrashield Magnet with an AVANCE III Console equipped with a BVT3000 variable temperature control unit. The measurements were performed at T = 37 °C to maintain a liquid crystalline phase (transition temperature of DMPC ∼24 °C). Lipid molecule dynamics were determined by ^{13}C NMR T_1 relaxation and steady-state NOE measurements,[48] which were used to extract local order parameters (S_{local}). The T_1 inversion recovery pulse sequence was used with recycle delay = 5 s, sufficient presaturation pulse strength = 1.5 kHz, and pulse length = 10 s. Interpulse delays ranged from 0.1 to 3 s. The T_1 inversion recovery data was fit with a three-parameter fit[53] to account for incomplete spin inversion. The steady-state NOE pulse sequence was used with a recycle delay = 5 s and presaturation pulse strength = 0 or 1.5 kHz with pulse length = 15 s. Continuous wave was used to saturate on the ^1H channel, and WALTZ-16 was used for proton decoupling at 3 kHz.

Data Fitting. To provide a thorough analysis of the segmental lipid dynamics at different degrees of curvature using ^{13}C NMR relaxation measurements in which couplings are not directly observed, we used an extension of the model-free approach[54] to evaluate the orientational local order parameters. In this method, a lipid molecule is free to rotate around its own principal axis, but the rotation around the other two axes is constrained by the bilayer architecture. In order to accurately describe this lipid motion, a squared order parameter for the entire lipid molecule, S_T^2, must be introduced, as well as a correlation time to describe the local motion, τ_T. Additionally, the overall correlation time must be considered, the inverse of which can be estimated as the sum of the inverse correlation times for the rotation of the beads in solution and the lateral diffusion of the lipids on the SiO_2 surface.[55] The magnitude of the estimated correlation times for the LCBs is too large to affect the spectral density function at the Larmor frequencies applied herein and are omitted in the evaluation of T_1 and NOE data.

With these assumptions in mind, the local order parameters were extracted from the raw data by fitting the T_1 and NOE data using the downhill method[55] in Matlab R2010a (The MathWorks, Inc.). Equation 3 was minimized to extract the values for S_{local} and τ_{local}, which are the order parameter and relaxation time for internal motion at each resolved carbon segment.[56,57] The T_1 relaxation time and the NOE factor (NOEF) are explicit functions of the spectral density, $J(\omega)$, which depends on S_{local} as follows.[56−58]

$$\text{error} = \sum_{\omega}\left(\frac{\text{NOE}_{calc} - \text{NOE}_{exp}}{\text{NOE}_{exp}}\right)^2 + \left(\frac{T_{1calc} - T_{1exp}}{T_{1exp}}\right)^2 \tag{3}$$

$$\frac{1}{T_1} = \frac{Nd^2}{4}[J(\omega_H - \omega_C) + 3J(\omega_C) + 6J(\omega_H + \omega_C)] \tag{4}$$

$$\text{NOEF} = 1 + \frac{Nd^2\gamma_H T_1}{4\gamma_C}[6J(\omega_H + \omega_C) - J(\omega_H - \omega_C)] \tag{5}$$

$$J(\omega) = \frac{2}{5}\left[\frac{(1 - S_T{}^2)S_{local}{}^2\tau_T}{1 + (\omega\tau_T)^2}\right] + \frac{2}{5}\left[\frac{(1 - S_{local}{}^2)\tau'}{1 + (\omega\tau')^2}\right] \tag{6}$$

where τ' reflects the correlation time of both the wobble and local motions and d is defined as follows, respectively:

$$\frac{1}{\tau'} = \frac{1}{\tau_T} + \frac{1}{\tau_{local}} \tag{7}$$

$$d = -\frac{\mu_0}{4\pi}\frac{\hbar\gamma_C\gamma_H}{r^3} = 1.2808 \times 10^5\ \text{s}^{-1} \tag{8}$$

In eqs 4−8, S_{local} and τ_{local} describe the order parameter and correlation time for local fast motions of the methylene C − H bond; S_T^2 and τ_T are the squared order parameter and correlation time for lipid wobble, respectively; N is the number of directly bound protons at a specific carbon site; ω_C and ω_H are the Larmor frequencies of ^{13}C and ^1H, respectively; γ_C and γ_H are the gyromagnetic ratios of ^{13}C and ^1H, respectively; and $\hbar$ is the reduced Planck's constant. The dipolar coupling constant was calculated using the vibrationally corrected value of r = 1.14 Å for the C−H bond.[59] The T_1 and NOE data obtained from both field strengths (ω/γ = 11.7 or 14.1 T) were fit by combining eqs 6−8 and eq 3. The value of S_T^2 was taken to be 0.34, and the value of τ_T was taken to be 1.9 ns.[58] S_T^2 was

DOI: 10.1021/jp510322t
J. Phys. Chem. B 2015, 119, 4194−4202

Table 1. DLS Analysis of SiO_2 Supports before and after Lipid Coating

bare SiO_2 beads		lipid coated beads		
size (nm)	polydispersity index	size (nm)	polydispersity index	bilayer thickness (calcd) (nm)
20.1 ± 1.4	0.090 ± 0.010	34.3 ± 3.0	0.070 ± 0.040	5.1 ± 1.2
31.5 ± 0.1	0.076 ± 0.014	45.3 ± 4.3	0.080 ± 0.050	4.9 ± 1.5
48.7 ± 2.0	0.080 ± 0.020	60.0 ± 2.0	0.071 ± 0.022	3.7 ± 0.9
63.2 ± 2.2	0.14 ± 0.03	75.6 ± 2.6	0.13 ± 0.02	4.2 ± 0.9
97.0 ± 3.4	0.078 ± 0.018	111.7 ± 3.6	0.086 ± 0.020	5.4 ± 1.8

considered a constant in order to extract the S_{local} and τ_{local} values reported herein. Variation of of S_T from 0.4 to 0.6 resulted in <10% change in the extracted values of S_{local} and τ_{local}.

RESULTS AND DISCUSSION

Materials Characterization. A comparison of the DLS results for both the bare SiO_2 beads and the LCBs are listed in Table 1. Each row in Table 1 reports the average size and the polydispersity index for the bare SiO_2 beads and the corresponding LCBs. The error bars listed in Table 1 represent standard deviations. On average, the beads are approximately 13.3 nm larger in diameter after coating. This observation qualitatively matches the value for the thickness of a DMPC bilayer (4.3 ± 0.2 nm) and the padding of the water layer (2 nm) between the SiO_2 surface and lipid bilayer head groups.[21,60] The DLS data were also used to estimate the bilayer thickness for each bead size (Table 1). Bilayer thickness was determined by taking half of the difference in diameter after lipid coating and subtracting 2 nm for the padding of the water layer. Percent error was determined by error propagation of the standard deviation in SiO_2 bead diameter and the standard deviation in LCB diameter, and was used to calculate the error in bilayer thickness. While all bilayer thickness values are within error of one another, the mean bilayer thicknesses for diameters between 60 and 80 nm LCBs appears slightly thinner than those of the other samples.

To confirm adsorption of a single bilayer on the SiO_2 beads, the samples were also analyzed by TGA. Table 2 shows that the

Table 2. TGA Analysis of Lipid Coated SiO_2 Beads

LCB size (nm)	calcd coverage (wt %)	exptl coverage (wt %)
34.3 ± 3.0	31.57	33.23 ± 0.10
45.3 ± 4.3	22.74	22.12 ± 0.08
60.0 ± 2.0	16.00	16.41 ± 0.08
75.6 ± 2.6	12.80	13.11 ± 0.13
111.7 ± 3.6	8.72	10.19 ± 0.17

experimental values are in good agreement with predicted values, assuming single bilayer lipid deposition onto the SiO_2 beads. Scanning electron microscopy (SEM) was collected for all raw SiO_2 beads before lipid coating to examine particle surfaces for changes in roughness for the SiO_2 nanoparticles (Supporting Information, Figure S1). The SEM results indicate that all SiO_2 beads were pseudospherical and exhibited no change in surface morphology as a function of diameter (consistent with the amorphous nature of SiO_2 materials), indicating that the underlying support was not manipulating bilayer properties. After thoroughly characterizing SiO_2 supports and LCBs, ^{13}C NMR relaxation measurements were performed to determine segmental lipid order parameters as a function of membrane curvature.

NMR Spectroscopy Measurements. ^{13}C NMR relaxation measurements were used to acquire dynamic information on DMPC molecules in the lipid bilayer for the different sized LCBs. For all curvature sizes and field strengths, the T_1 relaxation values generally increase as you move from the lipid headgroup down the acyl chain to the methyl terminus (Supporting Information, Figure S4A,B). The T_1 values for various curvature conditions are similar to one another within the error of the measurement. On the other hand, the NOE values are relatively similar for each carbon site on the lipid molecule (Supporting Information, Figure S4C,D). In general, at both 11.7 and 14.1 T, the NOE values are lowest for the 60 nm LCBs, while the NOE values for other curvature sizes are slightly higher, although the error at some positions is large. The variation in relaxation behavior for different samples is unlikely due to polydispersity, but could be from bilayer heterogeneity as a result of curvature or adsorption to a solid surface (vide infra). More insight could be gained from ^2H NMR spectroscopy measurements and/or MD simulations that can distinguish between *sn*-1 and *sn*-2 chains that are likely averaged in the relaxation measurements reported here. From the raw data, the local order parameters, S_{local}, as well as the local correlation times for individual carbon sites in DMPC for each curvature condition were obtained by fitting the ^{13}C T_1 and NOE data with eqs 3−8.

To confirm that the SiO_2 bead supports were not disrupting lipid bilayer formation and deposition, we also compared order parameters of the 110 nm LCBs with a those of a sample of unbound, monodisperse large unilamellar vesicles (LUVs) composed of DMPC with a diameter of 100 nm (Figure 2). The S_{local} values for carbon β, g_1, g_2, and g_3, and C3 were excluded because of the small signal-to-noise ratios and the large error that evolved from T_1 and NOE data during the fitting. It is important to note that, as bead size increased, the signal-to-noise ratio decreased due to slower tumbling. Therefore, for 110 nm LCBs and 100 nm LUVs, some

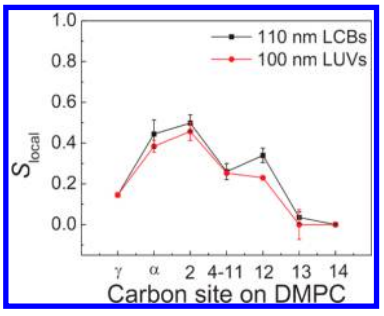

Figure 2. Local order parameter as a function of carbon position on the DMPC lipid molecule for LCBs (black squares) and LUVs (red circles) of similar sizes (d = 110 and 100 nm, respectively) are comparable, indicating that the SiO_2 bead support does not drastically alter the lipid dynamics.

DOI: 10.1021/jp510322t
J. Phys. Chem. B 2015, 119, 4194−4202

resonances with particularly low signal-to-noise (i.e., C2 and C12) exhibit larger errors in NOE factor, and the similarity in order parameter for these positions cannot be as certain (Supporting Information, Figure S4, Tables S5 and S6). Smaller diameter (extruded through 50 and 30 nm pore size polycarbonate membranes), unsupported DMPC vesicles were made to provide a more rigorous comparison of the effect of the SiO_2 beads, but were found to be unstable ~30 min after extrusion, prohibiting ^{13}C NMR relaxation measurements, which typically took a total of 12 h. Regardless, we found that the experimental order parameters for the 100 nm LUVs and 110 nm LCBs match well with each other and with previously reported NMR results,[57] as well as MD simulations of DMPC.[61,62]

The S_{local} values for all of the LCB samples are plotted in Figure 3, and the general pattern is consistent with previous

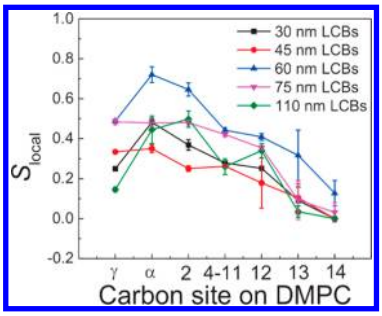

Figure 3. S_{local} as a function of carbon site on the DMPC molecule for 30 nm LCBs (black squares), 45 nm LCBs (red circles), 60 nm LCBs (blue up triangles), 75 nm LCBs (purple down triangles), and 110 nm LCBs (green diamonds).

reports.[57] From this data, two observations stand out: (i) the smaller sized LCBs (30 and 45 nm) show order parameter profiles similar to those of larger diameter (110 nm) LCBs and (ii) all of the values of S_{local} for intermediate sized (60 and 75 nm) LCBs are higher than those for other diameters of membrane curvature. Additionally, the local correlation times, τ_{local}, are plotted as a function of bead size in the Supporting Information, Figure S5. These values were found to be similar to those of previous reports for other lipid bilayer systems of similar sizes.[57] The local correlation times support that the dynamics of the 110 nm LCBs and 100 nm LUVs are similar to one another, while other sizes of LCBs show variation in lipid dynamics (vide infra).

In order to facilitate further comparison of the order parameters for specific carbon sites as a function of bead diameter, the local order parameters represented in Figure 3 are split into separate subplots as a function of carbon position in Figure 4. The subplots show the same trend for S_{local} dependence on diameter; it is typically below 0.5 for 30, 45, and 110 nm LCBs and 100 nm LUVs while the highest order parameter is generally found for diameters between 60 and 80 nm LCBs. Even in carbon segments where the ^{13}C NMR spectra exhibit a low signal-to-noise ratio (i.e., C13), the 60 nm LCBs still retain the highest order parameter within error.

Order Parameter Trends and Physical Properties of LCBs. For all LCB diameters, S_{local} follows the same general trend from the headgroup to the acyl chain. The choline headgroup (Cγ) begins at an intermediate order parameter, followed by an increase further down the headgroup (Cα). The S_{local} values dip just past the amphipathic portion of the headgroup (C2) at the start of the acyl chains, followed by a downward progression of the order parameter (C4–C11), with the most motional freedom observed at the end of the acyl chains (C12, C13, and C14). The order parameter profile is characteristic of hydrated lipid bilayers in which relative order is observed at the interfacial region due to tethering and alignment of the headgroup moieties and increased disorder is observed at the acyl chain termini.[63] The disorder associated with chain termini remains consistent throughout all degrees of curvature, indicating that the bilayer core maintains a constant degree of high motional freedom.

Chain termini disorder is consistent with previous work that examined the effect of acyl chain length on lipid segmental order parameter. It was noted that chain termini disorder remained consistent, while the headgroup and remaining acyl chain of the lipid molecule showed a strong dependence on chain length. The authors suggest that conclusions concerning

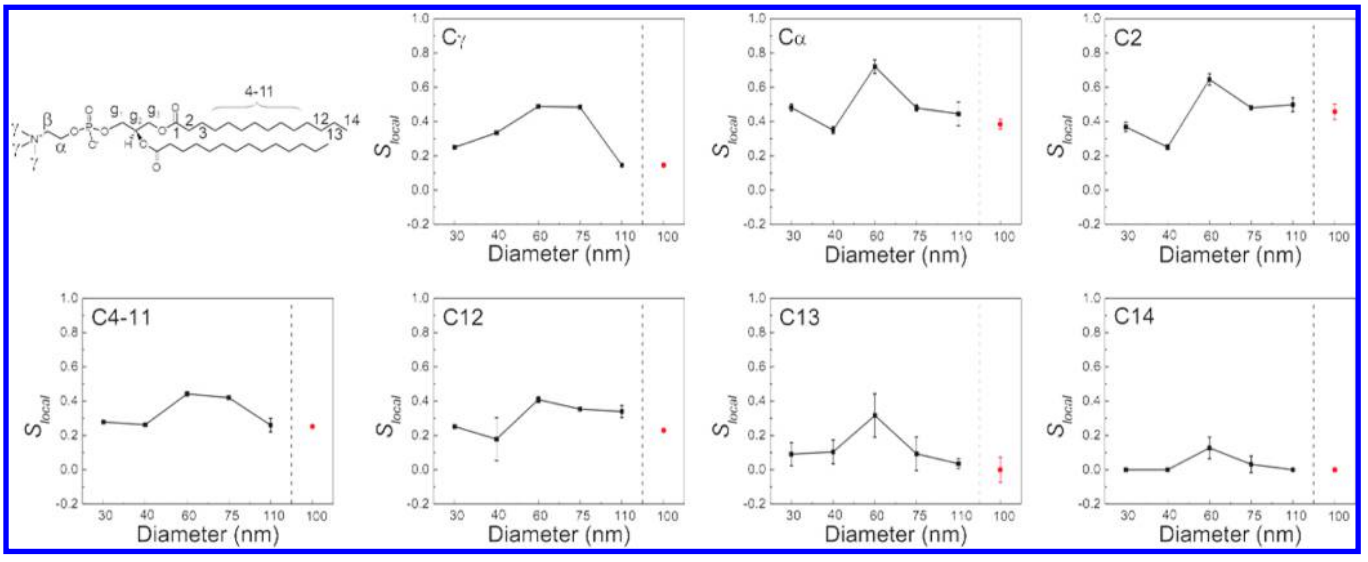

Figure 4. S_{local} as a function of carbon position on the lipid molecule for different diameter LCBs (black squares) compared to 100 nm LUVs (red circles). The intermediate sizes (60–80 nm LCBs) consistently display the highest value of S_{local}.

DOI: 10.1021/jp510322t
J. Phys. Chem. B 2015, 119, 4194–4202

the acyl chain dependence of differences in lipid structure and dynamics can be made simply based on analyzing the order parameter of the first two-thirds of the lipid molecule, starting at the headgroup.[63] Based on the data presented in Figure 3, it appears that this analysis can be extended to differences in curvature. In addition, Figure 4 shows that 60 nm LCBs maintain the highest S_{local} values for the entire lipid chain, indicating that structural differences are present at the acyl tails as well.

Increased Order Parameter Values at 60−80 nm and Physical Interpretation. Segmental order parameters for 30, 45, and 110 nm LCBs are generally similar to one another (Figure 4) despite large differences in membrane curvature. Curiously, an exception to this trend is observed at intermediate diameter LCBs (d = 60−80 nm), which consistently exhibit higher order parameters than other diameters. Two possibilities that can alter lipid molecule dynamics for intermediate diameter LCBs are explored: alterations in lipid hydration and interdigitation. Increased S_{local} has been demonstrated to be an effect of water exclusion from the bilayer, resulting in membrane stress and subsequent deformation, indicating that water plays a key role in membrane dynamics.[64] In fact, segmental lipid order parameter is so sensitive to changes in membrane hydration and osmotic pressure that previous work extracting order parameters of deuterated lipids suggests that NMR measurements can be used as an osmometer.[64] Specifically, for saturated lipids, such as DMPC, dehydration has been reported to result in an increased ordering of the upper two-thirds of the chains.[26] Membrane dehydration could further explain why S_{local} is significantly higher for the headgroup and top-to-middle region of the acyl chain for the 60 nm LCBs compared to other samples, while the terminal ends of the acyl chains remain consistently higher, but less dramatically so. Further, we can compare our values for S_{local} to previously reported values for the lipid order parameter, S_{CD}, measured with ^{2}H NMR spectroscopy as a function of membrane hydration by the following relationship:

$$S_{CD} = S_{local}S_T \quad (9)$$

Focusing on the interior methylenes (C4−C11), we found that our values for both small (30 and 45 nm) and large (110 nm) LCBs match well with those hydrated (~30−50 wt % H_2O), where $S_{CD} \sim 0.15$.[64] However, at intermediate sizes, the estimated value for $S_{CD} \sim 0.25$ according to eq 9 was more consistent with membranes containing ~7−10 wt % H_2O,[64] suggesting that curvatures with diameters between 60 and 80 nm exhibited a structural change that was consistent with membrane dehydration.

In addition to membrane dehydration, changes in S_{local} can also be the result of alterations in lipid hydrocarbon thickness and the average interfacial area per lipid molecule.[45] The phenomenon of increased S_{local} for intermediate sizes can also be indicative of a change in lipid bilayer packing structure, such as interdigitation.[65] As the lipid acyl chains become more intercalated with one another, the local motional freedom is restricted due to an increase in packing density, which is supported by the increase in S_{local} for even the acyl termini for 60 nm LCBs. The possibility of interdigitation is supported by a comparison of bilayer thicknesses that are calculated from DLS data (Table 1) before and after lipid deposition. A consequence of lipid interdigitation as a result of increased curvature is membrane thinning. As the membrane curvature becomes more pronounced, interdigitation occurs because of the necessity of avoiding the high free volume that would result from a bilayer structure of high curvature, leading to a decrease in membrane thickness. Membrane thinning is observed as curvature is increased during MD simulations due to lipid interdigitation.[19] Similar changes in membrane thickness and lateral order parameter were also observed in Raman spectroscopy studies for longer chain (C_{16} and C_{18}) PC spherical, supported lipid bilayers as a function of curvature.[20]

While Raman studies indicate that membrane thinning and interdigitation are observed at smaller diameters, small angle neutron scattering experiments on bilayers ranging from 184 to 62 nm in diameter indicate no change in bilayer thickness. However, thinning effects may not be present for unsaturated lipids until smaller diameters are reached.[66] Taken together, the DLS and order parameters measured here with ^{13}C NMR relaxation techniques show changes in the local order parameter as a function of membrane curvature that is consistent with lipid interdigitation for intermediate sizes (d = 60−80 nm). Other reports have used Fourier transform infrared (FTIR) spectroscopy and ^{2}H NMR to study lipid interdigitation in liquid crystalline DMPC bilayers in the presence of additives, such as phosphatidic acids.[65] This work presents the first evidence for membrane thinning and structural rearrangement such as interdigitation or alterations in membrane hydration measured with NMR for pure liquid crystalline DMPC bilayers as a function of curvature.

High Degrees of Curvature Order Parameter Analysis. As previously described, S_{local} for 30, 45, and 110 nm LCBs displays similar values despite the wide range of degrees of curvature. Values for S_{local} at both extreme ends of the curvature range measured in this study have already been reported for unsaturated phosphatidylcholine membranes using NMR relaxation.[57] Our work on fully saturated DMPC is consistent with the previously reported values for order parameters in unsaturated bilayers. Figure 5 shows a comparison of the order parameters we found for the interior methylenes on the acyl chain compared to previously reported values using NMR relaxation. The order parameters are generally consistent between both data sets, with the exception of the highest order parameter at intermediate sizes. The variation observed at 60−80 nm may be due to differences in the local order parameter of saturated lipids compared to unsaturated lipids, the observation of unique lipid dynamics that arise at intermediate sizes, or it may represent a change in membrane dynamics at high degrees of curvature that is obscured by

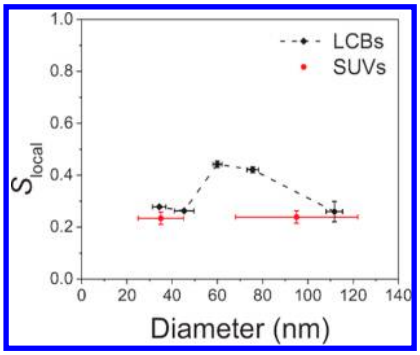

Figure 5. S_{local} values reported here for LCBs (black diamonds) are consistent with order parameters reported by Cafiso and co-workers[57] using NMR relaxation analyses examining small unilamellar vesicles (SUVs, red circles).

DOI: 10.1021/jp510322t
J. Phys. Chem. B 2015, 119, 4194−4202

population averaging in the NMR experiment. Indeed the first point is possible, since Raman spectroscopy indicates that variations in lipid chain length can cause alterations in the lateral order parameter for similar curvature sizes.[20]

While the similarity in order parameters between 30 and 110 nm LCBs can initially appear as a lack of difference between membrane structure and dynamics in this curvature range, the markedly different order parameter for all carbon sites at 60 nm seems to indicate that membrane dynamics do change with curvature. However, the differences in membrane thickness calculated from DLS data suggest that the structural changes between small and intermediate sizes are different from one another. In general, when considering the packing pattern of lipids supported on SiO_2 beads, the order parameters of each carbon segment will decrease with a decreased packing density.[67,68] Such differences in lipid packing patterns have been described with geometric models that account for molecular surface area and assume full volume occupancy.[69] For lipid molecules with moderately sized headgroups and saturated hydrocarbon chains, such as DMPC, a truncated cone geometry is predicted, indicating that some degree of membrane bending is energetically favorable. However, these simplified models do not allow for dynamics and are insufficient to describe molecular information because the surrounding environment is not accounted for, and solvation can play a significant role in membrane dynamics (vide supra). Regardless, it is possible that the lipid molecules are packing more densely at intermediate sizes, while less dense packing of lipids is found in 30, 45, and 110 nm LCBs. Changes in the order parameter due to packing differences as a function of curvature alone seem unlikely, since as the diameter of the bead approaches the size of the membrane, differences in packing for the inner and outer leaflets are expected to become more pronounced.

However, it is important to note that local order parameters represent a weighted average of the inner and outer leaflets. Attempts were made to distinguish between the inner and outer leaflets using paramagnetic ions to selectively dephase NMR signal from a single leaflet, but even minor alterations in the electrostatics resulted in DMPC aggregation and desorption of the bilayer from the SiO_2 support. Therefore, bilayer heterogeneity is averaged in the NMR measurements. At high degrees of curvature the inner leaflet is likely to be more tightly packed and the outer leaflet more loosely packed, resulting in an overall average order parameter that is weighted toward the leaflet with more lipid molecules. This population-weighted average order parameter for small diameters (30 and 45 nm) may be similar to S_{local} values observed for a bilayer with equally moderate packing for both leaflets, as is expected and observed at 110 nm. Order parameter averaging for the inner and outer leaflets of the lipid bilayer may explain the similarity in S_{local} values between 110 nm LCBs and 30−45 nm LCBs observed in NMR measurements.

CONCLUSIONS

We have demonstrated that the segmental order parameters of saturated lipid molecules in a bilayer do not vary continuously with bilayer curvature. For 60−80 nm LCBs, the DMPC molecules in the lipid bilayer show the highest values of S_{local}. Increasing interdigitation and/or membrane dehydration at intermediate curvature conditions may explain the changes in S_{local}, as well as the observation of membrane thinning. The results provide a useful model system to investigate the role of curvature in the propensity for small molecule additives and proteins to change or induce lipid interdigitation, and will likely produce unique findings for different lipids. The biological implications of dynamic lipid behavior at different degrees of curvature can be further assessed by modeling these interactions with computer simulations and further investigations with complementary techniques such as FTIR spectroscopy.

ASSOCIATED CONTENT

Supporting Information

SEM of raw SiO_2 beads, representative 1D ^{13}C NMR spectra, NOE and difference ^{13}C NMR spectra, and raw T_1 and NOE data. This material is available free of charge via the Internet at http://pubs.acs.org.

AUTHOR INFORMATION

Corresponding Author

*E-mail: lem64@pitt.edu. Tel.: 412-648-9917.

Author Contributions

L.E.M. and B.Y. contributed equally. The manuscript was written through contributions of all authors. All authors have given approval to the final version of the manuscript.

Notes

The authors declare no competing financial interest.

ACKNOWLEDGMENTS

This work was funded by NSF CAREER Award 0847417 and the University of Pittsburgh. We thank Profs. Lena Mäler and David Waldeck for helpful discussions. We thank Patrick Straney for collecting SEM images.

REFERENCES

(1) McMahon, H. T.; Gallop, J. L. Membrane Curvature and Mechanisms of Dynamic Cell Membrane Remodelling. *Nature* **2005**, *438*, 590−596.

(2) Mannella, C. A. Structure and Dynamics of the Mitochondrial Inner Membrane Cristae. *Biochim. Biophys. Acta, Mol. Cell Res.* **2006**, *1763*, 542−548.

(3) Parton, R. G.; Hanzal-Bayer, M.; Hancock, J. F. Biogenesis of Caveolae: A Structural Model for Caveolin-Induced Domain Formation. *J. Cell Sci.* **2006**, *119*, 787−796.

(4) Sanz-Herrera, J. A.; Moreo, P.; Garcia-Aznar, J. M.; Doblare, M. On the Effect of Substrate Curvature on Cell Mechanics. *Biomaterials* **2009**, *30*, 6674−6686.

(5) Shibata, Y.; Hu, J. J.; Kozlov, M. M.; Rapoport, T. A. Mechanisms Shaping the Membranes of Cellular Organelles. *Annu. Rev. Cell Dev. Biol.* **2009**, *25*, 329−354.

(6) Zimmerberg, J.; Kozlov, M. M. How Proteins Produce Cellular Membrane Curvature. *Nat. Rev. Mol. Cell Biol.* **2006**, *7*, 9−19.

(7) McHenry, A. J.; Sciacca, M. F. M.; Brender, J. R.; Ramamoorthy, A. Does Cholesterol Suppress the Antimicrobial Peptide Induced Disruption of Lipid Raft Containing Membranes? *Biochim. Biophys. Acta, Biomembr.* **2012**, *1818*, 3019−3024.

(8) Bhatia, V. K.; Hatzakis, N. S.; Stamou, D. A Unifying Mechanism Accounts for Sensing of Membrane Curvature by Bar Domains, Amphipathic Helices and Membrane-Anchored Proteins. *Semin. Cell Dev. Biol.* **2010**, *21*, 381−390.

(9) Markin, V. S.; Sachs, F. Thermodynamics of Mechanosensitivity. *Phys. Biol.* **2004**, *1*, 110−124.

(10) McIntosh, T. J.; Simon, S. A. Roles of Bilayer Material Properties in Function and Distribution of Membrane Proteins. *Annu. Rev. Biophys. Biomol.* **2006**, *35*, 177−198.

(11) Tian, A.; Baumgart, T. Sorting of Lipids and Proteins in Membrane Curvature Gradients. *Biophys. J.* **2009**, *96*, 2676−2688.

DOI: 10.1021/jp510322t
J. Phys. Chem. B 2015, 119, 4194−4202

(12) Brown, D. A.; London, E. Functions of Lipid Rafts in Biological Membranes. *Annu. Rev. Cell Dev. Biol.* **1998**, *14*, 111−136.
(13) Ikonen, E. Roles of Lipid Rafts in Membrane Transport. *Curr. Opin. Cell Biol.* **2001**, *13*, 470−477.
(14) Lingwood, D.; Simons, K. Lipid Rafts as a Membrane-Organizing Principle. *Science* **2010**, *327*, 46−50.
(15) Lucero, H. A.; Robbins, P. W. Lipid Rafts-Protein Association and the Regulation of Protein Activity. *Arch. Biochem. Biophys.* **2004**, *426*, 208−224.
(16) Mishra, S.; Joshi, P. G. Lipid Raft Heterogeneity: An Enigma. *J. Neurochem.* **2007**, *103*, 135−142.
(17) Munro, S. Lipid Rafts: Elusive or Illusive? *Cell* **2003**, *115*, 377−388.
(18) Pike, L. J. Lipid Rafts: Heterogeneity on the High Seas. *Biochem. J.* **2004**, *378*, 281−292.
(19) Risselada, H. J.; Marrink, S. J. Curvature Effects on Lipid Packing and Dynamics in Liposomes Revealed by Coarse Grained Molecular Dynamics Simulations. *Phys. Chem. Chem. Phys.* **2009**, *11*, 2056−2067.
(20) Ahmed, S.; Nikolov, Z.; Wunder, S. L. Effect of Curvature on Nanoparticle Supported Lipid Bilayers Investigated by Raman Spectroscopy. *J. Phys. Chem. B* **2011**, *115*, 13181−13190.
(21) Bayerl, T. M.; Bloom, M. Physical-Properties of Single Phospholipid-Bilayers Adsorbed to Micro Glass-Beads—a New Vesicular Model System Studied by H-2-Nuclear Magnetic-Resonance. *Biophys. J.* **1990**, *58*, 357−362.
(22) Brown, M. F.; Thurmond, R. L.; Dodd, S. W.; Otten, D.; Beyer, K. Elastic Deformation of Membrane Bilayers Probed by Deuterium NMR Relaxation. *J. Am. Chem. Soc.* **2002**, *124*, 8471−8484.
(23) Davis, J. H. The Description of Membrane Lipid Conformation, Order and Dynamics by ^{2}H NMR. *Biochim. Biophys. Acta* **1983**, *737*, 117−171.
(24) Douliez, J. P.; Leonard, A.; Dufourc, E. J. Restatement of Order Parameters in Biomembranes: Calculation of C-C Bond Order Parameters from C-D Quadrupolar Splittings. *Biophys. J.* **1995**, *68*, 1727−1739.
(25) Dufourc, E. J.; Parish, E. J.; Chitrakorn, S.; Smith, I. C. P. Structural and Dynamical Details of Cholesterol-Lipid Interaction as Revealed by Deuterium NMR. *Biochemistry* **1984**, *23*, 6062−6071.
(26) Gawrisch, K.; Holte, L. L. NMR Investigations of Non-Lamellar Phase Promoters in the Lamellar Phase State. *Chem. Phys. Lipids* **1996**, *81*, 105−116.
(27) Labbé, J.-F.; Cronier, F.; C.-Gaudreault, R.; Auger, M. Spectroscopic Characterization of DMPC/DOTAP Cationic Liposomes and Their Interactions with DNA and Drugs. *Chem. Phys. Lipids* **2009**, *158*, 91−101.
(28) Macquaire, F.; Bloom, M. Membrane Curvature Studied Using Two-Dimensional NMR in Fluid Lipid Bilayers. *Phys. Rev. E* **1995**, *51*, 4735−4742.
(29) Oldfield, E.; Meadows, M.; Rice, D.; Jacobs, R. Spectroscopic Studies of Specifically Deuterium Labeled Membrane Systems. Nuclear Magnetic Resonance Investigation of Effects of Cholesterol in Model Systems. *Biochemistry* **1978**, *17*, 2727−2740.
(30) Seelig, J. Deuterium Magnetic Resonance: Theory and Application to Lipid Membranes. *Q. Rev. Biophys.* **1977**, *10*, 353−418.
(31) Seelig, J.; Waespesarcevic, N. Molecular Order in Cis and Trans Unsaturated Phospholipid Bilayers. *Biochemistry* **1978**, *17*, 3310−3315.
(32) Stockton, G. W.; Smith, I. C. P. A Deuterium Nuclear Magnetic Resonance Study of the Condensing Effect of Cholesterol on Egg Phosphatidylcholine Bilayer Membranes. I. Perdeuterated Fatty Acid Probes. *Chem. Phys. Lipids* **1976**, *17*, 251−263.
(33) Stockton, G. W.; Johnson, K. G.; Butler, K. W.; Tulloch, A. P.; Boulanger, Y.; Smith, I. C. P.; Davis, J. H.; Bloom, M. Deuterium NMR Study of Lipid Organization in Acholeplasma Laidlawii Membranes. *Nature* **1977**, *269*, 267−268.
(34) Urbina, J. A.; Pekerar, S.; Le, H.-b.; Patterson, J.; Montez, B.; Oldfield, E. Molecular Order and Dynamics of Phosphatidylcholine Bilayer Membranes in the Presence of Cholesterol, Ergosterol and Lanosterol: A Comparative Study Using ^{2}H-, ^{13}C- and ^{31}P-NMR Spectroscopy. *Biochim. Biophys. Acta, Biomembr.* **1995**, *1238*, 163−176.
(35) Dvinskikh, S. V.; Castro, V.; Sandstrom, D. Probing Segmental Order in Lipid Bilayers at Variable Hydration Levels by Amplitude- and Phase-Modulated Cross-Polarization NMR. *Phys. Chem. Chem. Phys.* **2005**, *7*, 3255−3257.
(36) Gross, J. D.; Warschawski, D. E.; Griffin, R. G. Dipolar Recoupling in MAS NMR: A Probe for Segmental Order in Lipid Bilayers. *J. Am. Chem. Soc.* **1997**, *119*, 796−802.
(37) Urbina, J. A.; Moreno, B.; Arnold, W.; Taron, C. H.; Orlean, P.; Oldfield, E. A Carbon-13 Nuclear Magnetic Resonance Spectroscopic Study of Inter-Proton Pair Order Parameters: A New Approach to Study Order and Dynamics in Phospholipid Membrane Systems. *Biophys. J.* **1998**, *75*, 1372−1383.
(38) Warschawski, D. E.; Devaux, P. F. Order Parameters of Unsaturated Phospholipids in Membranes and the Effect of Cholesterol: A H-1-C-13 Solid-State NMR Study at Natural Abundance. *Eur. Biophys. J.* **2005**, *34*, 987−996.
(39) Yamamoto, K.; Soong, R.; Ramamoorthy, A. Comprehensive Analysis of Lipid Dynamics Variation with Lipid Composition and Hydration of Bicelles Using Nuclear Magnetic Resonance (NMR) Spectroscopy. *Langmuir* **2009**, *25*, 7010−7018.
(40) Andersson, A.; Mäler, L. Magnetic Resonance Investigations of Lipid Motion in Isotropic Bicelles. *Langmuir* **2005**, *21*, 7702−7709.
(41) Brown, M. F.; Ribeiro, A. A.; Williams, G. D. New View of Lipid Bilayer Dynamics from ^{2}H and ^{13}C NMR Relaxation Time Measurements. *Proc. Natl. Acad. Sci. U. S. A.* **1983**, *80*, 4325−4329.
(42) Varner, S. J.; Vold, R. L.; Hoatson, G. L. Characterization of Molecular Motion in the Solid State by Carbon-13 Spin−Lattice Relaxation Times. *J. Magn. Reson.* **2000**, *142*, 229−240.
(43) Lindahl, E.; Edholm, O. Molecular Dynamics Simulation of NMR Relaxation Rates and Slow Dynamics in Lipid Bilayers. *J. Chem. Phys.* **2001**, *115*, 4938−4950.
(44) Pastor, R. W.; Venable, R. M.; Karplus, M.; Szabo, A. A Simulation Based Model of NMR T_1 Relaxation in Lipid Bilayer Vesicles. *J. Chem. Phys.* **1988**, *89*, 1128−1140.
(45) Petrache, H. I.; Tu, K.; Nagle, J. F. Analysis of Simulated NMR Order Parameters for Lipid Bilayer Structure Determination. *Biophys. J.* **1999**, *76*, 2479−2487.
(46) Leftin, A.; Brown, M. F. An NMR Database for Simulations of Membrane Dynamics. *Biochim. Biophys. Acta, Biomembr.* **2011**, *1808*, 818−839.
(47) Andersson, A.; Mäler, L. Size and Shape of Fast-Tumbling Bicelles as Determined by Translational Diffusion. *Langmuir* **2006**, *22*, 2447−2449.
(48) Lind, J.; Nordin, J.; Mäler, L. Lipid Dynamics in Fast-Tumbling Bicelles with Varying Bilayer Thickness: Effect of Model Transmembrane Peptides. *Biochim. Biophys. Acta, Biomembr.* **2008**, *1778*, 2526−2534.
(49) Grage, S.; Heinz, S.; Bayerl, T. M. Diffusion of Lipids in Supported Bilayers as an NMR Probe for Topological Studies in Nanoporous Solids. *Eur. Biophys J.* **1998**, *27*, 425−428.
(50) Linseisen, F. M.; Hetzer, M.; Brumm, T.; Bayerl, T. M. Differences in the Physical Properties of Lipid Monolayers and Bilayers on a Spherical Solid Support. *Biophys. J.* **1997**, *72*, 1659−1667.
(51) Ahmed, S.; Wunder, S. L. Effect of High Surface Curvature on the Main Phase Transition of Supported Phospholipid Bilayers on SiO_2 Nanoparticles. *Langmuir* **2009**, *25*, 3682−3691.
(52) Savarala, S.; Ahmed, S.; Ilies, M. A.; Wunder, S. L. Formation and Colloidal Stability of DMPC Supported Lipid Bilayers on SiO2 Nanobeads. *Langmuir* **2010**, *26*, 12081−12088.
(53) Levy, G. C.; Peat, I. R. The Experimental Approach to Accurate Carbon-13 Spin-Lattice Relaxation Measurements. *J. Magn. Reson. (1969−1992)* **1975**, *18*, 500−521.
(54) Lipari, G.; Szabo, A. Model-Free Approach to the Interpretation of Nuclear Magnetic Resonance Relaxation in Macromolecules. 1. Theory and Range of Validity. *J. Am. Chem. Soc.* **1982**, *104*, 4546−4559.

DOI: 10.1021/jp510322t
J. Phys. Chem. B 2015, 119, 4194−4202

(55) Bocian, D. F.; Chan, S. I. NMR Studies of Membrane Structure and Dynamics. *Annu. Rev. Phys. Chem.* **1978**, *29*, 307−335.
(56) Ellena, J. F.; Lepore, L. S.; Cafiso, D. S. Estimating Lipid Lateral Diffusion in Phospholipid Vesicles from Carbon-13 Spin-Spin Relaxation. *J. Phys. Chem.* **1993**, *97*, 2952−2957.
(57) Lepore, L. S.; Ellena, J. F.; Cafiso, D. S. Comparison of the Lipid Acyl Chain Dynamics Between Small and Large Unilamellar Vesicles. *Biophys. J.* **1992**, *61*, 767−775.
(58) Allerhan, A.; Doddrell, D.; Komorosk, R. Natural Abundance Carbon-13 Partially Relaxed Fourier Transform Nuclear Magnetic Resonance Spectra of Complex Molecules. *J. Chem. Phys.* **1971**, *55*, 189−&.
(59) Brown, M. F. Theory of Spin-Lattice Relaxation in Lipid Bilayers and Biological Membranes. Dipolar Relaxation. *J. Chem. Phys.* **1984**, *80*, 2808−2831.
(60) Johnson, S. J.; Bayerl, T. M.; Mcdermott, D. C.; Adam, G. W.; Rennie, A. R.; Thomas, R. K.; Sackmann, E. Structure of an Adsorbed Dimyristoylphosphatidylcholine Bilayer Measured with Specular Reflection of Neutrons. *Biophys. J.* **1991**, *59*, 289−294.
(61) Takaoka, Y.; Pasenkiewicz-Gierula, M.; Miyagawa, H.; Kitamura, K.; Tamura, Y.; Kusumi, A. Molecular Dynamics Generation of Nonarbitrary Membrane Models Reveals Lipid Orientational Correlations. *Biophys. J.* **2000**, *79*, 3118−3138.
(62) Vermeer, L. S.; de Groot, B. L.; Reat, V.; Milon, A.; Czaplicki, J. Acyl Chain Order Parameter Profiles in Phospholipid Bilayers: Computation from Molecular Dynamics Simulations and Comparison with ^{2}H NMR Experiments. *Eur. Biophys J.* **2007**, *36*, 919−931.
(63) Petrache, H. I.; Dodd, S. W.; Brown, M. F. Area Per Lipid and Acyl Length Distributions in Fluid Phosphatidylcholines Determined by ^{2}H NMR Spectroscopy. *Biophys. J.* **2000**, *79*, 3172−3192.
(64) Mallikarjunaiah, K. J.; Leftin, A.; Kinnun, J. J.; Justice, M. J.; Rogozea, A. L.; Petrache, H. I.; Brown, M. F. Solid-State ^{2}H NMR Shows Equivalence of Dehydration and Osmotic Pressures in Lipid Membrane Deformation. *Biophys. J.* **2011**, *100*, 98−107.
(65) Ziegler, W.; Blume, A. Acyl Chain Conformational Ordering of Individual Components in Liquid-Crystalline Bilayers of Mixtures of Phosphatidylcholines and Phosphatidic Acids. A Comparative FTIR and ^{2}H NMR Study. *Spectrochim. Acta, Part A* **1995**, *51*, 1763−1778.
(66) Kucerka, N.; Pencer, J.; Sachs, J. N.; Nagle, J. F.; Katsaras, J. Curvature Effect on the Structure of Phospholipid Bilayers. *Langmuir* **2007**, *23*, 1292−1299.
(67) Dill, K. A.; Flory, P. J. Interphases of Chain Molecules: Monolayers and Lipid Bilayer Membranes. *Proc. Natl. Acad. Sci. U. S. A.* **1980**, *77*, 3115.
(68) Huang, C.; Mason, J. Geometric Packing Constraints in Egg Phosphatidylcholine Vesicles. *Proc. Natl. Acad. Sci. U. S. A.* **1978**, *75*, 308.
(69) Israelachvili, J. N. *Intermolecular and Surface Forces*; Academic Press: Waltham, MA, 2010.

DOI: 10.1021/jp510322t
J. Phys. Chem. B 2015, 119, 4194−4202